IEEE Journal of Translational Engineering in Health and Medicine

Received 30 December 2016; revised 22 March 2017 and 3 May 2017; accepted 7 May 2017.
Date of publication July 7, 2017; date of current version August 4, 2017.

Digital Object Identifier 10.1109/JTEHM.2017.2708100

Seismocardiography-Based Cardiac Computed Tomography Gating Using Patient-Specific Template Identification and Detection

JINGTING YAO[1], (Student Member, IEEE), SRINI TRIDANDAPANI[2], (Senior Member, IEEE), CARSON A. WICK[2], (Member, IEEE), AND PAMELA T. BHATTI[1], (Member, IEEE)

[1]School of Electrical and Computer Engineering, Georgia Institute of Technology, Atlanta, GA 30332-0250, USA
[2]Department of Radiology and Imaging Sciences, Emory University, Atlanta, GA 30032, USA

CORRESPONDING AUTHOR: PAMELA T. BHATTI (pamela.bhatti@ece.gatech.edu)

This work was supported in part by the National Science Foundation under Grant CAREER ECCS-1055801 and in part by the National Center for Advancing Translational Sciences, National Institutes of Health, under Award UL1TR000454. The work of S. Tridandapani and C. A. Wick was supported by the National Institute of Biomedical Imaging and Bioengineering under Award K23EB013221.

ABSTRACT To more accurately trigger cardiac computed tomography angiography (CTA) than electrocardiography (ECG) alone, a sub-system is proposed as an intermediate step toward fusing ECG with seismocardiography (SCG). Accurate prediction of quiescent phases is crucial to prospectively gating CTA, which is susceptible to cardiac motion and, thus, can affect the diagnostic quality of images. The key innovation of this sub-system is that it identifies the SCG waveform corresponding to heart sounds and determines their phases within the cardiac cycles. Furthermore, this relationship is modeled as a linear function with respect to heart rate. For this paper, B-mode echocardiography is used as the gold standard for identifying the quiescent phases. We analyzed synchronous ECG, SCG, and echocardiography data acquired from seven healthy subjects (mean age: 31; age range: 22–48; males: 4) and 11 cardiac patients (mean age: 56; age range: 31–78; males: 6). On average, the proposed algorithm was able to successfully identify 79% of the SCG waveforms in systole and 68% in diastole. The simulated results show that SCG-based prediction produced less average phase error than that of ECG. It was found that the accuracy of ECG-based gating is more susceptible to increases in heart rate variability, while SCG-based gating is susceptible to high cycle to cycle variability in morphology. This pilot work of prediction using SCG waveforms enriches the framework of a comprehensive system with multiple modalities that could potentially, in real time, improve the image quality of CTA.

INDEX TERMS Cardiac gating, cardiac quiescence, computed tomography angiography (CTA), coronary angiography, echocardiography, electrocardiography (ECG), seismocardiography (SCG).

I. INTRODUCTION

A. MOTIVATION AND BACKGROUND

According to the American Heart Association, cardiovascular disease (CVD) is the leading cause of death in the United States. More than 2150 Americans lose their lives to CVD everyday, one every 40 seconds on average [1]. The gold standard for evaluating CVD is catheter coronary angiography (CCA). This method requires X-ray visualization of arterial blockages while dye is released into the bloodstream through catheters placed in the coronary arteries. Despite its clinical prevalence, CCA has inherent limitations. It is an invasive technique with a non-negligible complication rate [2] and is relatively expensive [1]. Also, while it visualizes the coronary arterial lumen, it does not directly provide information about vessel wall abnormalities [3]. As an emerging alternative, computed tomography angiography (CTA), is increasingly being used for the evaluation of coronary arteries, and can provide information for the vessel wall [4]. CTA evaluation is less invasive, faster, and less expensive [5], [6]. Moreover, it does not suffer from catheter-related complications such as bleeding, stroke, or heart attack [2], [7]. However, CTA performance is limited by temporal resolution and consequently can suffer from artifacts caused by cardiac motion. Therefore, it is crucial to obtain

2168-2372 © 2017 IEEE. Translations and content mining are permitted for academic research only.
Personal use is also permitted, but republication/redistribution requires IEEE permission.
See http://www.ieee.org/publications_standards/publications/rights/index.html for more information.

cardiac imaging data during the periods of the cardiac cycle when the heart motion is minimized. Those quasi-stationery periods are referred to as quiescent periods or phases during which the CT machine is triggered, or gated, for data acquisition. The ultimate goal of this work is to improve the diagnostic quality while also reducing the radiation dose of CTA.

Many studies have been undertaken with the goal of improving the accuracy of CTA gating to increase the diagnostic yield of CTA [9]–[12]. Since the inception of cardiac CTA, quiescent phase prediction has relied almost exclusively on the real-time electrocardiography (ECG) signal. CTA data acquisition is triggered by either a prospective gating signal derived from that ECG signal, or by retrospectively selecting CTA data from ECG-selected phases [13], [14]. Specifically, a pre-defined linear piecewise function predicting the quiescent phase with respect to heart rate is often employed [15]–[18]. This approach neglects the intra- and inter-personal variation in cardiac signals with respect to the cardiac motion and thus is not always reliable. Also, the previously published papers provide several different versions of these gating functions, suggesting that ECG-based gating lacks standardization leaving room for substantial improvement. Furthermore, while providing important information as to the electrical activity during the cardiac cycle, ECG gating fails to inherently capture the mechanical motion of the heart. As an alternative, echocardiography, which directly evaluates cardiac motion in real time, was previously demonstrated to provide more accurate gating timing [19], [20] for CTA, and thus can be used as a baseline for quiescence. However, echocardiography has some disadvantages, including incompatibility with CTA in real-time since current clinically available transducers can cause streak artifacts in the CTA images [10].

Seismocardiography (SCG) is a noninvasive strategy to record the low-frequency vibration caused by the heart motion by placing an accelerometer on the chest wall [23]. The accelerometer uses a smaller footprint than the echocardiography transducer, thus significantly minimizing streak artifacts [10], and is less expensive. Additionally, SCG is not operator dependent during data acquisition. Crow *et al.* [24] evaluated the relationship between SCG and echocardiography and reported consistency between the timing of phases of these two modalities, which indicates their similar accuracy in measuring cardiac time intervals. The current advances in SCG signal processing include but are not limited to the identification of quiescent heart phases [9], [11], extraction of respiratory and cardiac gating information [25], and delineation of the SCG signal [26], [27].

Further comparison between SCG and echocardiography [24], [28]–[30] suggested that SCG can reliably capture cardiac motion and therefore potentially be a supplement to ECG in CTA gating (Fig. 1). Multiple signal processing techniques including frequency analysis, time series regression [31] and wavelet transform [32] have been applied to

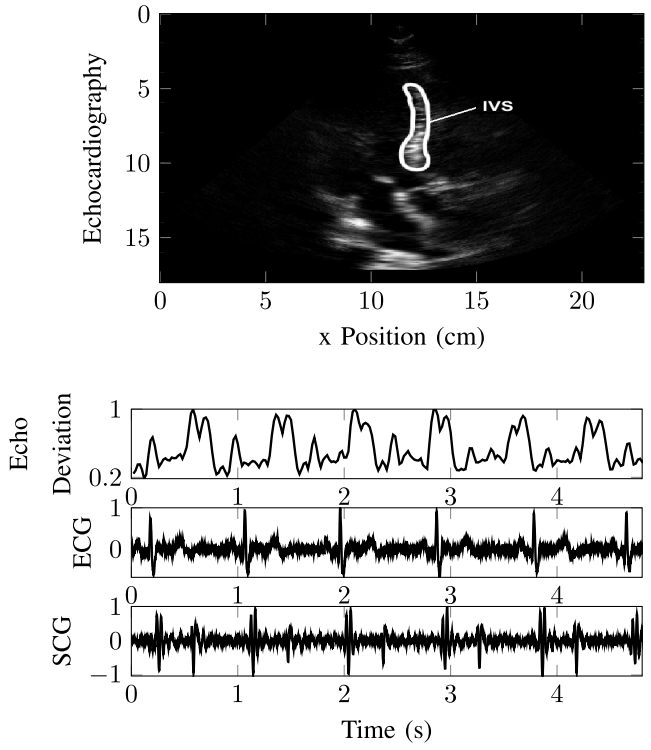

FIGURE 1. Echocardiography: B-mode echocardiography frame from an apical four chamber view of the heart, with contour shown around the inter-ventricular septum (IVS); Echo Deviation: Motion signals calculated from B-mode sequences by applying the phase-to-phase deviation measure elaborated in [8]; ECG: Time-series de-noised ECG signal; SCG: Time-series de-noised SCG signal.

ECG signals for cardiac research, but the exploration of fusing SCG with ECG to optimize cardiac gating for CTA has not been attempted thus far. We propose to fuse SCG and ECG to optimize cardiac gating for CTA. As an intermediate stage, we propose to detect the prominent signal features of the SCG that are associated with two heart sounds ($S1$ and $S2$), denoted as $SS1$ and $SS2$ [22], [33], as illustrated in Fig. 2, with a proposed template matching approach due to the similarity of their morphology across heart beats. Based on the detected features, we find the relationship between the timing of cardiac events and heart rate using template matching and detection, and subsequently propose a fused framework to predict quiescent phases based on ECG and SCG. Average templates of SCG waveforms associated with $S1$ and $S2$ are generated using a windowed selection method over the training data. Then, by matching the average templates with SCG waveform throughout all cardiac cycles in the testing data, the waveforms of $SS1$ and $SS2$ are identified by a template matching approach. The ultimate goal of this work is to generate personalized and cohort (group consisting of either healthy subjects or cardiac patients) gating functions based on SCG along with ECG to more accurately predict quiescent phases to trigger CTA gating.

Traditionally, a waveform nomenclature-based approach to identify cardiac events is not robust because the SCG markers

IEEE Journal of Translational Engineering in Health and Medicine

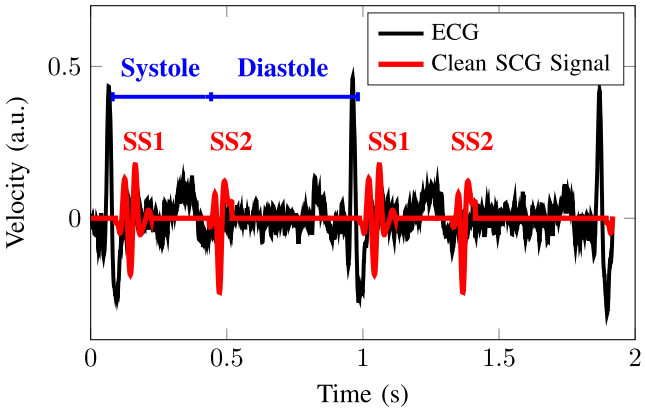

FIGURE 2. Plot of de-noised ECG and SCG wave packets associated with heart sounds *S*1 and *S*2, denoted as *SS*1 and *SS*2, respectively, from clean SCG signal. Heart sounds are discrete bursts of auditory vibrations that vary in intensity, frequency, quality and duration [21]. By placing an accelerometer on the sternum, the first and second heart sounds can be detected [22]. The first heart sound (*S*1) is caused by the closure of atrio-ventricular valves; the second heart sound (*S*2) is from the closure of semilunar valves [22]. *S*1 leads the onset of systolic period while *S*2 occurs after the systolic period and precedes the diastolic period.

such as aortic opening and mitral closure are not consistent if solely following the template indices [25], [34]; and there is no universal identification template that would work for signals from all patients. The automatic annotation approach for SCG proposed in [35] shows accurate identification, but only on healthy subjects. Therefore, template annotation can be nontrivial and complicated. The proposed template detection and identification algorithm for SCG is able to accurately recognize the occurrence of cardiac events, and the relationship between the cardiac events are delineated with a linear fit. Also, using echocardiography as the ground truth, a voting mechanism is designed to select from two potential quiescent phases based on their stability. A patient-specific phase delay function indicating the phase delay from the waveform associated with heart sound to the following quiescent phase is generated as a linear function with respect to heart rate. The phase delay function, along with the detected heart sound waveform and predicted heart rate, are combined together to predict the quiescent phase.[1]

The goal of this work is to establish a framework for development of a robust technique to predict in real-time, for each heartbeat, whether ECG- or SCG-derived quiescence leads to more diagnostic coronary CTA. This study is critical in providing the basis for development of the hardware for real-time prediction of quiescence. Ultimately, this will improve the diagnostic quality of coronary CTA. This is particularly important for patients with a low pretest probability of disease since they can avoid invasive CCA and its associated costs and risks. At the same time, such a technique can also lead to reduced radiation dose with coronary CTA since retrospective gating can be avoided.

[1]To clarify the nomenclature used in the cardiac gating community, the following definitions are used. Cardiac quiescence is a state of minimal motion, defined relative to the overall motion over the cardiac cycle. A cardiac quiescent period is an interval of time when the heart is considered quiescent. A cardiac quiescent phase is a specific phase (percentage) of the cycle, suitable for triggering CT acquisition.

B. PAPER ORGANIZATION

The rest of this paper is organized as follows. Section II describes subjects and data acquisition, and elaborates on the template identification and detection approach for *SS*1 and *SS*2. The voting mechanism to identify quiescent phase for echocardiography, and the method to predict quiescence on a beat-by-beat basis with SCG are also addressed in Section II as well the the methodology for comparing the performance of ECG and SCG is described for eventual use in SCG and ECG fusion. The results and analysis are provided in Section III. Lastly, a discussion is given in Section IV including limitations and future work.

II. METHODS AND PROCEDURES

A schematic system diagram is shown in Fig. 3 where each block is described in the following subsections. Subject and data acquisition is described below. B-mode echocardiography is used as the gold standard for identifying the quiescent phases. To find quiescence as a function of heart rate, a voting mechanism for echocardiography as described in Section II-B models the optimal quiescence-heart rate relationship in the form of a linear fit $P_{ECHO}(r) = a_{ECHO} \cdot r + b_{ECHO}$, where $P_{ECHO}(r)$ is the quiescent phase defined in echocardiography at heart rate r, a_{ECHO} is the slope and b_{ECHO} is the intercept. The technical methods to detect heart sound-associated waveforms and to determine their timings are elaborated in Section II-C. The timings are recognized in terms of phases in the cardiac cycles and a linear fit, $P_{SCG}(r) = a_{SCG} \cdot r + b_{SCG}$, is used to describe the relationship of the cardiac events in SCG, where $P_{SCG}(r)$ is the phase of the waveform defined in SCG at heart rate r, a_{SCG} is the slope and b_{SCG} is the intercept. Linear fit is used due to its simplicity in modeling, and it was demonstrated in this work that linear function is a suitable choice. Therefore, the phase delay from the heart sound-associated waveform to its corresponding quiescent phase is a linear function with respect to heart rate. Section II-D provides a detailed explanation of the phase delay function $P_{Delay}(r) = P_{ECHO}(r) - P_{SCG}(r)$. Heart rate prediction is described in Section II-F. With the linear association of delay in the occurrence of cardiac events ($P_{Delay}(r)$), given a predicted heart rate ($\hat{r}$) and a timing of heart sound of a cardiac cycle in SCG (P_{SCG}), the corresponding quiescent phase of the current cardiac cycle ($P_{SCG}(\hat{r})$) can be predicted. This predicted timing allows for comparisons with the timing calculated from ECG gating function. Section II-G gives a detailed description of the training and testing methods. Performance metrics for comparisons are specified in Section II-H.

A. SUBJECTS AND DATA ACQUISITION

Data acquisition was approved by the Emory University Institutional Review Board with written consent obtained from each participant. Seven healthy subjects (mean age: 31; age range: 22-48; males: 4) and eleven patients with

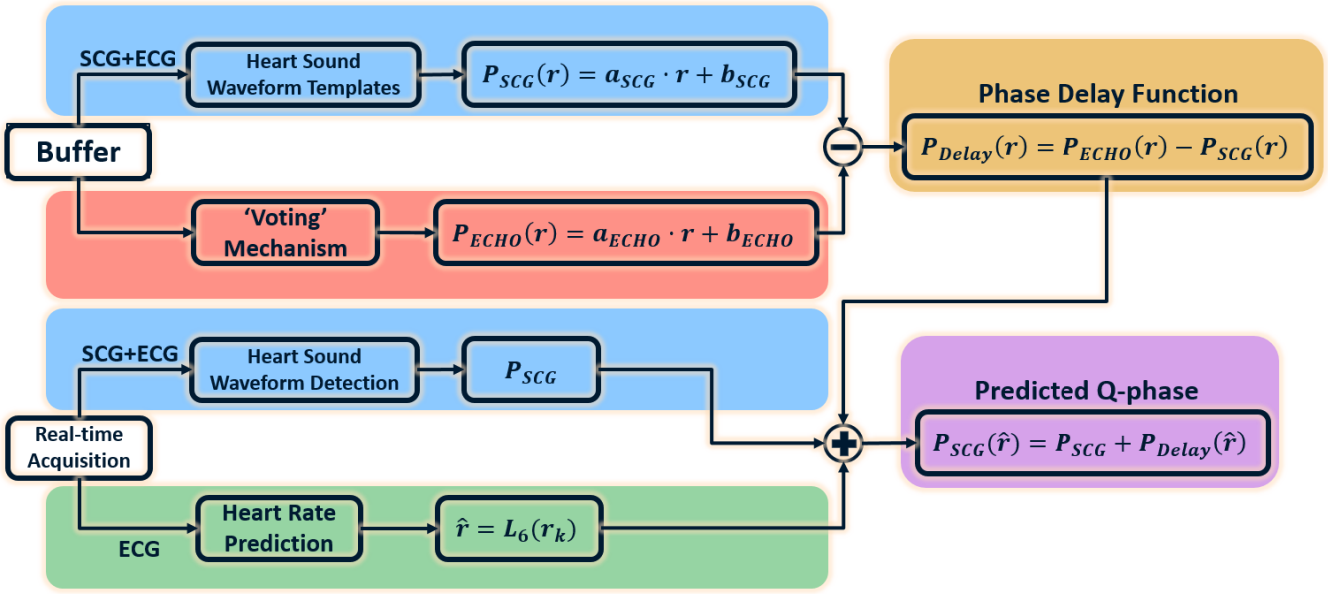

FIGURE 3. Schematic system diagram outlining SCG and ECG-based prediction. The upper part of the diagram uses training data to generate the phase delay function (Section II-D) supported by the heart sound-associated waveform detection of SCG (Section II-C) and voting mechanism of echocardiography (Section II-B). The lower part uses testing data to recognize the phase of current heart sound-associated waveform and predict the current heart rate (Section II-F). Eventually, the quiescent phase is predicted with the joint information of the training and testing data (Section II-G).

valvular or structural heart disease (mean age: 56; age range: 31-78; males: 6) participated in data acquisition.[2] Data used in this study was acquired using a custom SCG device and a commercial ultrasound machine simultaneously. The ultrasound machine used was a SonixTOUCH Research Scanner (Analogic, Peabody, MA, USA). Details of the ECG-SCG and ECG-echocardiography acquisition device systems are described in [10]. During data acquisition, the subjects were resting in supine position for a least five minutes. A one dimensional accelerometer, the SCG device, recording in the dorso-ventral direction was placed against the sternum, perpendicular to the skin surface, and acceleration was recorded at a rate of 1.2 kHz. B-mode echocardiography data obtained via the apical four-chamber view was recorded at a rate of 50 Hz. Simultaneously, the ECG data on the ultrasound machine was acquired at a rate of 200 Hz. The ECG signals from the two devices were used to align the SCG and echocardiography signals, and also to segment cardiac cycles.

B. B-MODE ECHOCARDIOGRAPHY BASELINE

B-mode echocardiography is used as the gold standard for identifying the quiescent phases. Motion signals are representations of approximated magnitude of the velocity of coronary vessels, which has been shown in the past to be approximated by the motion of the interventricular septum [36]. Cardiac motion magnitude is calculated from B-mode sequences by applying the phase-to-phase deviation measure elaborated in [8]. R-R intervals of the synchronized ECG are used to segment the one dimensional motion-based signals and are used to define cardiac phases (%). Systolic and diastolic quiescent phases are characterized as phases with the least velocity in the systolic (with center before 60%) and diastolic (with center after 60%) periods of a cardiac cycle, respectively. Wick *et al.* [9] demonstrated a linear relationship between the delay from SCG-to-echocardiography-detected phases with respect to heart rate.

A linear relationship was each observed between the quiescent phases of the SCG and echocardiography with respect to heart rate. To condense the cardiac signal information into slope and intercept and compare to those results from the piece-wise constant function of ECG, this work is conducted with the assumption that there exists a linear relationship between quiescent phase and heart rate. However, the traditional approach to identify the lowest point within a certain search range is not robust enough to identify the same feature. There could be more than one potential minima that meet the requirement of being a quiescent phase. A voting mechanism is designed to select the most stable point in both systole and diastole. Within both quiescent periods of a cardiac cycle for each subject, the quiescent phases were identified on a beat-by-beat basis by implementing a voting mechanism in which two candidate quiescent phases of least velocity within each cardiac cycle were recognized in the first round, forming two groups of quiescent phases dependent on heart rate. The quiescent phases are expected to be in a linear relationship with respect to heart rate, as it is reported in [9]. In the second round of voting, the total least squares residuals calculated by

[2]Originally, data was acquired from eleven healthy subjects and eleven patients with valvular or structural heart disease. But the data acquired from four of the healthy subjects were either noisy or incomplete for this study because the data acquisition system was not sophisticated enough at the initial stage of data gathering, so only seven of the subsequently obtained healthy subjects' data were analyzed in this study.

IEEE Journal of Translational Engineering in Health and Medicine

forming a linear fit of data in each group were compared and the group with less residual was considered as more robust and therefore quiescent phases in this group were selected as the most optimal phases for gating within the quiescent period.

C. TEMPLATE IDENTIFICATION AND GENERATION

Different morphologies in a cardiac signal correspond to specific physiological events in the cardiac cycle. For example, the high frequency accelerometric components of SCG are associated with the heart sounds [22]. We study the relationship between the timing of two waveforms associated with heart sound and their corresponding quiescent phases in systole and diastole.

The annotation approach [35] to identify the cardiac events of SCG is nontrivial and unstable due to the large variation in inter- and intra-personal cardiac signals. This study proposes to use the waveforms of the heart sounds and applies a template matching approach to detect the occurrence of heart sounds in real time for predicting the quiescent phases. Raw data is pre-processed to obtain a cleaner signal for later steps. To reduce the noise and interference components, the SCG signal is first conditioned with a low-pass filter (f_c = 20 Hz) [37], and then passed through a notch filter centered at 0 Hz with a cutoff of approximately 2 Hz to remove the DC component and respiratory baseline wander in the signal. The frequency range of the noise signal was determined from the signal spectrum in the frequency domain. The redundancy of the ECG signals from the custom SCG acquisition device and the ultrasound machine are used to temporally synchronize across the three modalities. The ECG signal recorded from the custom SCG acquisition device is low-pass filtered with a cutoff of 50 Hz to remove the high frequency content. Similarly, the ECG signal recorded from the ultrasound machine is passed through a low-pass filter with a cutoff of 30 Hz. Both the resulting ECG signals from the custom device and the ultrasound machine are filtered with the same notch filter as described for SCG.

The synchronized R-R intervals of the ECG were used to segment the conditioned SCG signals into cardiac cycles. To extract the waveforms associated with the first and second heart sounds, temporal windows containing the two waveforms individually are designed based on statistics from previous studies on the occurrence of heart sounds [21], [38]. Normally, $S1$ component is lower in frequency and lasts for a longer duration than $S2$ component [21]. The average duration of $S1$ and $S2$ components are approximately 0.13 second and 0.08 second, respectively [38]. Because our custom-built device synchronously acquires data at a rate of 1.2 kHz, the searching windows in systole and diastole are 160 and 100 samples long, respectively. In prior work, the timing of quiescent periods was studied by analyzing SCG signals from seven healthy subjects and eleven patients with valvular or structural cardiac disease [11]. It was found that on average, the center of systolic and diastolic quiescent periods were at 29% and 76% for healthy subjects, and 33% and 79% for patients with cardiovascular disease. Accordingly, the search range of the two waveforms were set from S_{start} = 1% to S_{end} = 30% and D_{start} = 30% to D_{end} = 65% for healthy subjects, and 1% to 33% and 33% to 79% for the cardiac patients. The procedures for identifying each waveform ($SS1$ and $SS2$) and generating the corresponding waveform template consisted of the following steps:

1) Extract the waveform associated with the heart sound with the aforementioned windowed searching approach in each cardiac cycle. For a specific subject, denote the the waveform from the i-th cardiac cycle $w(i)$, $i = 1, \ldots, N$.
2) Use the longest waveform as the reference length, zero padding the rest of the waveforms to be equal length to the reference length, and obtain the composite waveform $\bar{w} = \frac{1}{N}\sum_{i=1}^{N} w(i)$.
3) Apply Hilbert transform to obtain an upper (e_{upper}) and lower envelope (e_{lower}) around the composite waveform. The composite envelope is the difference between the two envelopes $\bar{w}_d = e_{upper} - e_{lower}$ [22].
4) Find the time position τ_P, in terms of sample index in the composite waveform, of the peak of the difference envelope. Then, the time delay from the start of the previous R-peak to the τ_P is $\tau_{PR} = \tau_P + \bar{L} * search_{start}$, where $search_{start} = S_{start}$ or D_{start} and $\bar{L}$ is the average cycle length.
5) Recapture waveform associated with heart sound by extracting waveform around τ_{PR} in each cardiac cycle and τ_{PR} being the center of the window and with the window details the same as aforementioned.
6) Generate the waveform template by averaging the recaptured waveform, normalized to unit energy.

The ensemble average in step 2) and 3) reduces the noise and artifacts, and the composite waveform can be used to robustly determine the optimal peak of the heart sound waveform on average. The difference envelope increases the time resolution in detecting the optimal peak of the high frequency waveform. Any real signal $s(t)$ can be written uniquely in the form $s(t) = e(t)cos(2\pi f_c t + \theta(t))$ where $e(t)$ is the envelope and $\theta(t)$ is the phase of $s(t)$. The relationship of the signal and its Hilbert transform is $\tilde{s}(t) = \frac{1}{\sqrt{2}} e(t) e^{j\theta(t)}$. It is noted that the Hilbert transform was originally defined for periodic functions. The waveform associated with the two heart sounds in this study are sinusoidal-like (and thus quasi-periodic), so the Hilbert transform works well in finding their envelopes. However, the Hilbert transform may not be able to accurately capture the envelopes of some random waveform. The upper and lower envelope, as well as the difference envelope are shown in Fig. 4. The peak of the difference envelope indicates the time position corresponding to the peak of the waveform. Steps 1) - 4) approximately capture waveform of the high frequency components of the heart sounds; step 5) more accurately captures the optimal peak location τ_{PR}.

Figure 2 shows an example of the SCG signal after synthesizing the SCG with the waveform template. This is achieved by convolving the waveform template with the con-

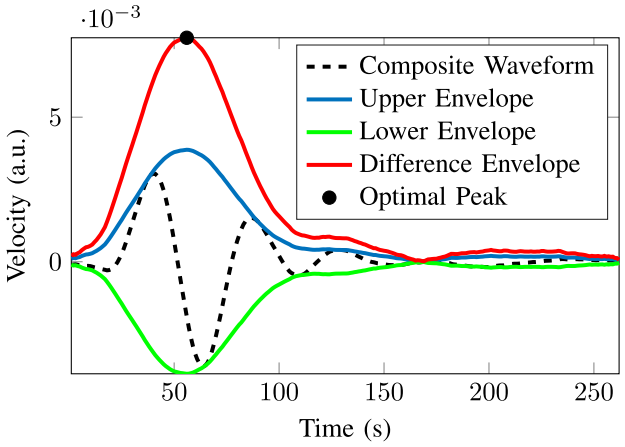

FIGURE 4. Example of the composite envelope and the difference envelope which is the difference between the upper and lower envelope formed using Hilbert transform. The peak of the difference envelope is considered the optimal peak of the composite waveform.

ditioned SCG; the peak of convolved result locates the center of $SS1$ and $SS2$. Ideally, after convolution, each cardiac cycle should have one peak indicating the center of waveform in systole and one in diastole. However, the conditioned SCG signal can still be distorted and noisy, whereby peaks may be absent or occur in the wrong phase of the cardiac cycle. The false peaks outside the searching range $[S_{start}, S_{end}]$ for systole or $[D_{start}, D_{end}]$ for diastole are filtered out. In this case, the waveform detection and identification algorithm does not provide an optimal output if it fails in locating the waveform suggesting the need for fusing ECG and SCG.

D. PHASE DELAY FUNCTION

For computational efficiency, the phase delay function is a linear function with respect to heart rate that characterizes the time relationship between the peak of waveform associated with heart sound waveform in SCG and the quiescent phase in echocardiography in each cardiac cycle. More formally, the phase delay functions for systole and diastole can be represented by:

$$P^{Sys}_{Delay}(r) = P^{Sys}_{ECHO}(r) - P^{Sys}_{SCG}(r), \tag{1}$$

$$P^{Dias}_{Delay}(r) = P^{Dias}_{ECHO}(r) - P^{Dias}_{SCG}(r), \tag{2}$$

where $P^{Sys}_{SCG}(r)$ and $P^{Dias}_{SCG}(r)$ are phases of the peak of the waveform in systole ($SS1$) and diastole ($SS2$), respectively, for heart rate r. $P^{Sys}_{ECHO}(r)$ and $P^{Dias}_{ECHO}(r)$ are quiescent phases in systole and diastole obtained from echocardiography. The phase delay function arises since the waveform associated with heart sound in SCG occurs, and can be detected, earlier than the quiescent phase in echocardiography.

It has been discussed in Section II-B that a linear function can be used to describe the relationship of quiescent phases with respect to heart rate. Similarly, the timing of the waveforms in the SCG with respect to heart rate can also be modeled using a linear function. For both of the linear functions, SCG heart sound waveform and echocardiography quiescent phase with respect to heart rate, an outlier removal technique was applied to get an unbiased linear function. Outlier removal is applied to both the detected phases and heart rate. For phases in the linear function, any sample which strays away from the linear fit by more than two standard deviations was removed. For heart rates, any sample which strays away from the average heart rate by more than three standard deviation was removed. A new linear fit is constructed after removing the outliers.[3]

E. ECG GATING FUNCTION

Currently, cardiac CTA is triggered by ECG, specifically, a predefined piece-wise constant gating function relying upon a predicted heart rate. Previous literature has extensively studied the optimal systolic and diastolic reconstruction intervals for ECG-based CTA using retrospective analysis. This work selectively uses a very comprehensive gating function from [15],

$$P_{ECG}(\hat{r}) = \begin{cases} 65\% & \hat{r} \leq 60 \text{ bpm}, \\ 75\% & 60 \text{ bpm} < \hat{r} \leq 70 \text{ bpm}, \\ 85\% & 70 \text{ bpm} < \hat{r} \leq 83 \text{ bpm}, \\ 35\% & \hat{r} > 83 \text{ bpm}. \end{cases} \tag{3}$$

where $\hat{r}$ is the predicted heart rate. P_{ECG} is the delay, in terms of phase of the cardiac cycle (% interval within the cycle), from the start of the most recent R peak of the ECG to the start of the quiescent period.

As an important aside, the given function provides the phase of the triggering signal with respect to the beginning of the systolic and diastolic quiescent phases rather than the center of the acquisition window. A linear conversion was made to the gating function which becomes a heart-rate-dependent piece-wise function. The retrospective cardiac CTA data were acquired using a Siemens Somatom Definition dual-source 64-sliece CT Scanner (Siemens Corp., Erlangen, Germany) whose reconstruction window length is 83ms.

F. HEART RATE PREDICTION

The heart rates corresponding to six prior heart beats can be used to predict the upcoming heart rate [39]. In this study, a linear regression with six previous samples gives the least mean square error (MSE) in predicting the next instantaneous heart rate as compared to polynomial fit of other forms and autoregressive (AR) model. The mathematical model can be expressed as

$$r_n = L_6(r_i) = \sum_{i=n-6}^{n-1} \beta_n r_i + \epsilon_n, \tag{4}$$

where r_n is the current heart rate to be predicted, r_i is the previous heart rate with index i, and ϵ_n is the n-th noise term, that is, random error. Linear regression is a useful linear

[3]The cardiac phases have more natural variance as compared to heart rates, and so the outlier remover for phases was set to have a tighter range of tolerance.

model that can be applied to real-valued time series to recognize the pattern of a set of samples and thus is an appropriate model in predicting the instantaneous heart rate.

G. TRAINING AND TESTING

For each subject, the synchronized ECG and SCG data are divided into two parts. Inspired by machine learning, the data used for generating the phase delay function is called *training* data. The data used to generate the predicted quiescent phase of the SCG is called the *testing* data. Again, following the rule of thumb from machine learning, the ratio of training and testing data is 4 to 1 [39]. The training and testing data are exclusive independent continuous cardiac cycles. The testing data is used to predict the quiescent phase, and compare the SCG predicted quiescent phase with that calculated from the ECG gating function. The synchronized raw ECG and SCG data were pre-processed first as described in Section II-C.

Whereas the training data are used to generate the phase delay function, the testing data are used to predict the quiescent phase on a beat-by-beat basis. For each patient, using the patient-specific template waveform generated by the algorithm described in Section II-C, the current waveform can be identified and its timing with respect to the most adjacent previous R-peak, denoted as t_{SCG} (sec), can be identified. The heart rate prediction algorithm presented in Section II-F provides the predicted heart rate $\hat{r}$ (bpm) for the current cardiac cycle. The phase of the current waveform is $P^w_{SCG} = t_{SCG} \cdot \hat{r}/60$. Therefore, the predicted quiescent phase from SCG is $P_{SCG}(\hat{r}) = P^w_{SCG} + P_{Delay}(\hat{r})$ where $P_{Delay}(\hat{r})$ is calculated as described in Section II-D from the training data.

H. PERFORMANCE METRICS

For each subject, the first and second heart sound-associated waveforms were identified on a beat-by-beat basis using the proposed waveform identification method elaborated in Section II-C. For those cardiac cycles in which heart sound-associated waveforms are not identified, the default is to apply what is predicted by the ECG algorithm.

There are two ways to evaluate the performance of SCG prediction. One is to use patient-specific phase delay functions, and the other is to use cohort-specific approach for prediction. Within each cohort, for a specific subject/patient, an average phase delay function can be generated with the information of the rest of the subjects in the same cohort. In cohort-specific approach, the population is split between two cohorts, one is the healthy subjects population, the other is the heart disease patients population. The average phase delay function is the difference between the average echocardiography quiescent phase function ($P_{ECHO}(r)$) and the average SCG heart sound waveform phase function ($P^w_{SCG}(r)$), that is,

$$\bar{P}_{Delay}(r) = \bar{P}_{ECHO}(r) - \bar{P}^w_{SCG}(r), \tag{5}$$

$$\bar{P}_{ECHO}(r) = \frac{1}{N-1}\sum_j P_{ECHO}(r_j), \tag{6}$$

$$\bar{P}^w_{SCG}(r) = \frac{1}{N-1}\sum_j P^w_{SCG}(r_j), \tag{7}$$

where j is the index of the subjects/patients exclusive of the current subject of study. N is the cardinality of the cohort of study. The phase error is defined as the absolute difference between the predicted quiescent phase and the echocardiography baseline quiescent phase,

$$E_{SCG}(r_n) = |P_{SCG}(\hat{r}_n) - P_{ECHO}(r_n)|, \tag{8}$$

or,

$$E_{ECG}(r_n) = |P_{ECG}(\hat{r}_n) - P_{ECHO}(r_n)|, \tag{9}$$

where n is the index of a specific cardiac cycle; r_n represents the true heart rate and $\hat{r}_n$ is the predicted heart rate. The predicted quiescent phase is obtained on a beat-by-beat basis in a simulated real-time scenario; the baseline quiescent phase is obtained from the echocardiography linear function against true heart rate. Heart rate error is the numerical difference between the true heart rate and the predicted heart rate,

$$E_{HR}(r_n) = r_n - \hat{r}_n, \tag{10}$$

The average heart rate error for a specific subject is the mean of the absolute value of the heart rate values:

$$\bar{E}_{HR} = \frac{1}{N}\sum_{n=1}^{N} |E_{HR}(r_n)|, \tag{11}$$

For each subject, the average phase error is the mean of all the phase error over all the testing cardiac cycles, and the heart rate variation is the variation of heart rate over the testing data,

$$\bar{E}_{SCG} = \frac{1}{N}\sum_{n=1}^{N} E_{SCG}(\hat{r}_n), \tag{12}$$

or,

$$\bar{E}_{ECG} = \frac{1}{N}\sum_{n=1}^{N} E_{ECG}(\hat{r}_n), \tag{13}$$

$$var_{HR} = \frac{1}{N}\sum_{n=1}^{N} (r_n - \mu_{HR})^2, \tag{14}$$

The following four metrics are examined:

1) Waveform identification rate: The percentage of valid waveforms that are identified within the training data range of each subject. This measures the robustness of the proposed waveform identification algorithm.
2) The variation of phase error along with the change of heart rate.
3) The change of phase error against the heart rate error.
4) The overall phase error versus heart rate variation.

III. RESULTS

Two forms of evaluation are presented. The first is generated with the patient-specific phase delay function. The second is with the phase delay function obtained in each cohort with application of leave-one-out method. The summarized statistics in TABLE 1 are shown graphically in Fig. 6 to Fig. 10. The calculated average phase errors and overall results of all

TABLE 1. Error statistics.

Healthy Subjects								
Subject	Avg HR (bpm)	HRV (ms)	Average Phase Error (%) / Absolute Average Error (millisecond)					
			Personalized SCG		Cohort SCG		ECG	
			Systole	Diastole	Systole	Diastole	Systole	Diastole
1	58	41	3.30 ± 5.26	5.50 ± 6.01	4.75 ± 4.07	6.62 ± 4.18	-	5.84 ± 4.06
			30.76 ± 48.77	52.36 ± 6.01	52.03 ± 50.75	62.12 ± 41.20	-	56.16 ± 42.30
2	60	48	1.5 ± 2.38	2.54 ± 4.40	4.23 ± 1.94	8.61 ± 2.96	5.73 ± 3.37	4.89 ± 3.13
			13.06 ± 23.67	22.47 ± 4.4	37.06 ± 23.18	70.27 ± 21.97	43.23 ± 20.18	42.47 ± 27.63
3	68	28	2.94 ± 4.99	3.46 ± 6.34	2.43 ± 4.04	6.12 ± 4.80	10.62 ± 10.61	6.07 ± 3.88
			25.22 ± 40.96	30.66 ± 6.34	22.39 ± 33.58	54.91 ± 33.31	63.81 ± 55.47	56.22 ± 35.65
4	73	50	2.36 ± 4.74	2.72 ± 3.66	4.44 ± 4.78	2.46 ± 4.13	3.25 ± 3.81	9.15 ± 2.72
			18.99 ± 39.27	21.76 ± 3.66	36.82 ± 40.28	17.95 ± 30.60	31.66 ± 52.76	74.2 ± 23.83
5	77	50	2.00 ± 2.48	1.70 ± 3.20	3.06 ± 2.07	4.04 ± 3.67	11.37 ± 2.94	7.77 ± 3.16
			14.59 ± 19.45	11.97 ± 3.2	21.84 ± 16.19	24.66 ± 21.00	76.16 ± 14.57	59.45 ± 27.19
6	84	19	2.40 ± 3.96	0.92 ± 2.45	5.56 ± 1.47	2.78 ± 2.80	8.82 ± 0.88	5.30 ± 1.03
			17.25 ± 28.20	6.71 ± 2.45	39.7 ± 8.28	18.51 ± 14.18	62.36 ± 5.02	38.86 ± 8.48
7	92	58	0.88 ± 0.94	1.68 ± 1.31	5.10 ± 1.79	4.83 ± 2.23	3.55 ± 1.23	7.68 ± 0.47
			6.04 ± 6.05	11.41 ± 1.31	34.55 ± 11.95	32.11 ± 13.49	23.37 ± 6.92	53.82 ± 5.25
Avg	72	42	2.20	2.65	4.23	5.07	7.22	6.67
	72	42	17.99	22.48	34.91	40.08	50.1	54.45
σ	12	13	0.82	1.50	1.11	2.20	3.54	1.55
	12	13	8.12	15.5	10.42	21.89	20.59	11.6

Cardiac Patients								
Subject	Avg HR (bpm)	HRV (ms)	Average Phase Error (%) / Absolute Average Error (millisecond)					
			Personalized SCG		Cohort SCG		ECG	
			Systole	Diastole	Systole	Diastole	Systole	Diastole
8	52	20	2.11 ± 3.31	9.69 ± 11.17	1.95 ± 3.23	11.24 ± 6.01	2.51 ± 2.08	14.66 ± 3.22
			22.90 ± 35.23	107.36 ± 11.17	22.36 ± 35.05	124.19 ± 69.68	22.14 ± 16.45	157.34 ± 25.00
9	54	65	1.21 ± 1.71	5.45 ± 6.29	1.85 ± 1.52	10.91 ± 4.59	-	17.91 ± 4.47
			13.1018.30	59.516.29	20.4514.52	120.8456.24	-	192.7242.73
10	54	208	2.84 ± 3.42	4.59 ± 4.1	6.16 ± 3.28	13.4 ± 3.77	1.22 ± 0.4	10.82 ± 0.85
			19.11 ± 2.40	31.33 ± 4.1	32.054.15	21.76 ± 7.40	8.11 ± 2.46	76.22 ± 10.06
11	63	63	2.08 ± 3.42	2.81 ± 4.1	3.09 ± 3.28	6.77 ± 3.77	-	3.64 ± 3.06
			19.72 ± 32.19	26.97 ± 4.1	28.79 ± 29.41	62.33 ± 30.45	-	34.47 ± 27.08
12	64	38	2.22 ± 2.22	4.27 ± 3.4	2.68 ± 2.03	3.48 ± 4.79	-	7.75 ± 1.29
			18.2218.03	35.14 ± 3.4	21.7 ± 16.36	25.08 ± 30.10	-	63.64 ± 11.41
13	65	60	4.47 ± 2.56	5.92 ± 7.4	0.05 ± 2.39	9.75 ± 8.90	3.08 ± 1.12	8.93 ± 4.54
			38.79 ± 19.39	52.12 ± 7.4	24.51 ± 15.26	66.85 ± 71.45	31.56 ± 15.53	76.43 ± 41.73
14	73	57	3.34 ± 3.37	2.89 ± 5.2	13.09 ± 3.63	11.64 ± 4.20	14.96 ± 0.8	0.2 ± 0.41
			24.68 ± 25.26	21.38 ± 5.20	96.15 ± 27.08	84.78 ± 29.35	108.36 ± 3.44	1.48 ± 2.33
15	81	170	3.59 ± 5.1	15.37 ± 14.33	3.27 ± 4.64	12.05 ± 13.12	13.74 ± 13.68	11.54 ± 8.64
			31.87 ± 49.61	141.55 ± 14.33	31.09 ± 49.62	95.59 ± 115.28	91.58 ± 75.69	96.26 ± 78.36
16	84	147	2.98 ± 3.54	9.47 ± 9.67	28.31 ± 4.48	11.98 ± 7.43	18.46 ± 0.42	11.6 ± 1.93
			21.15 ± 25.54	67.98 ± 9.67	201.48 ± 36.33	76.87 ± 53.61	131.32 ± 17.54	81.42 ± 16.18
17	87	29	2.57 ± 4.17	6.31 ± 5.74	2.13 ± 4.03	12.28 ± 6.18	2.45 ± 0.73	16.59 ± 2.9
			18.38 ± 29.91	44.69 ± 5.74	15.21 ± 28.96	85.6 ± 45.63	17.16 ± 5.90	123.13 ± 26.06
18	102	3	3.67 ± 1.84	0.48 ± 0.37	12.01 ± 2.91	27.92 ± 0.61	0.51 ± 0.12	-
			20.92 ± 10.54	2.76 ± 0.37	67.58 ± 14.58	159.48 ± 3.65	2.95 ± 0.74	-
Avg	70	78	2.76	5.95	6.82	11.34	7.12	10.37
	70	78	22.62	53.71	51.03	83.94	51.65	90.31
σ	16	66	0.94	4.21	8.16	6.18	7.28	5.52
	16	66	7.11	40.15	55.5	41.19	50.55	56.06

subjects are summarized numerically in TABLE 1 with the phase errors presented both as patient specific, and in terms of their cohort. The corresponding errors in time (millisecond) are also presented. Note that the cardiac cycles where wave packet detection failed were omitted, and therefore were not included in the calculation of phase errors. On average, the average phase errors of SCG-based prediction in systole and diastole are 5.53% and 8.21%, respectively, and 7.17% and 8.52% with ECG-based prediction. In TABLE 2 and TABLE 3, the two cohorts, healthy subjects and cardiac disease patients, are further grouped based on their heart rates, as low heart rate (<75 beats per minute) or high heart rate (≥75 beats per minute). The numerical value provides the average phase error and standard deviation of that group. In the subsections below, selective plots of individuals are shown, and plots of average absolute phase error calculated with patient-specific and cohort phase delay function are presented (Fig. 6 to Fig. 10).

Note that in TABLE 1, there are average phase errors in systole that do not apply to ECG. This is because for each predicted heart rate, there is only one predicted quiescent phase from ECG, which is either in systole or diastole. For subject 1, especially when the heart rate is low, all the predicted quiescent phases lie in the diastole. So this subject

TABLE 2. Average error calculated with patient-specific phase delay function.

		$\bar{E}_{SCG}^{systole}$ (%)	$\bar{E}_{SCG}^{diastole}$ (%)	$\bar{E}_{ECG}^{systole}$ (%)	$\bar{E}_{ECG}^{diastole}$ (%)
		Absolute Average Error (millisecond)			
Healthy Subjects	Low HR (<75 bpm)	2.52 ± 0.78	3.55 ± 1.35	6.53 ± 3.75	6.48 ± 1.84
		22.01 ± 7.66	31.81 ± 14.28	46.23 ± 16.28	57.26 ± 13.01
	High HR (≥ 75 bpm)	1.76 ± 0.78	1.43 ± 0.44	7.91 ± 3.98	6.91 ± 1.40
		12.63 ± 5.86	10.03 ± 2.89	53.97 ± 27.38	50.71 ± 10.64
Cardiac Patients	Low HR (<75 bpm)	2.61 ± 1.05	4.94 ± 2.34	5.44 ± 6.39	9.13 ± 6.08
		22.36 ± 8.12	47.6929.63	42.5444.93	86.0467.03
	High HR (≥ 75 bpm)	3.20 ± 0.52	7.90 ± 6.21	8.79 ± 8.96	13.24 ± 2.89
		23.08 ± 6.00	64.24 ± 58.17	60.75 ± 61.02	100.27 ± 21.14

TABLE 3. Average error calculated with the cohort-specific phase delay function.

		$\bar{E}_{SCG}^{systole}$ (%)	$\bar{E}_{SCG}^{diastole}$ (%)	$\bar{E}_{ECG}^{systole}$ (%)	$\bar{E}_{ECG}^{diastole}$ (%)
		Absolute Average Error (millisecond)			
Healthy Subjects	Low HR (<75 bpm)	3.96 ± 1.04	5.95 ± 2.56	6.53 ± 3.75	6.48 ± 1.84
		37.07 ± 12.10	51.31 ± 23.11	46.23 ± 16.28	57.26 ± 13.01
	High HR (≥ 75 bpm)	4.57 ± 1.33	3.88 ± 1.03	7.91 ± 3.98	6.91 ± 1.40
		32.03 ± 9.19	25.09 ± 6.81	53.97 ± 27.38	50.71 ± 10.64
Cardiac Patients	Low HR (<75 bpm)	4.12 ± 4.36	9.59 ± 3.37	5.44 ± 6.39	9.13 ± 6.08
		35.14 ± 27.22	72.26 ± 41.06	42.54 ± 44.93	86.04 ± 67.03
	High HR (≥ 75 bpm)	11.43 ± 12.08	16.06 ± 7.90	8.79 ± 8.96	13.24 ± 2.89
		82.60 ± 103.26	86.02 ± 9.37	60.75 ± 61.02	100.27 ± 21.14

only has phase errors in diastole. From TABLE 2 which shows results generated from the patient-specific phase delay function, the SCG-based prediction demonstrated less average phase error and standard deviation among all subjects, while ECG gives more average phase error and variance in all groups in TABLE 2. TABLE 3 shows results generated from the cohort phase delay function. With increasing heart rate, the phase error increases for both healthy subjects and cardiac patients. For healthy subjects, SCG-based prediction caused less average phase error than ECG both in systole and diastole. For cardiac patients, particularly with high heart rate, SCG-based prediction in both systole and diastole produced slightly more average phase errors than ECG. The second waveform resulted in the largest average phase error in both cohorts, for low and high heart rates. Also of note, the phase error standard deviation is much higher for cardiac patients, in particular patients with high heart rate.

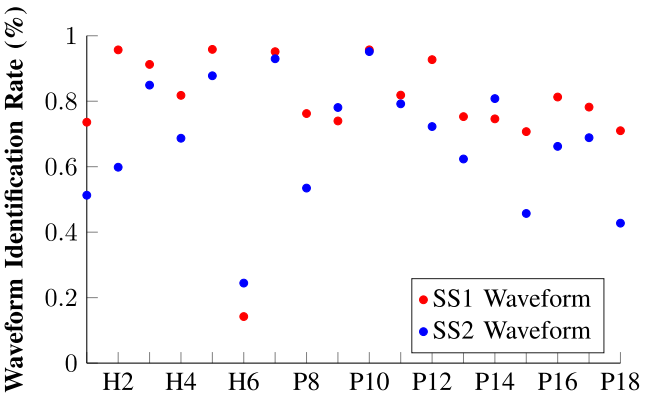

FIGURE 5. Waveform identification rate. The first seven scatter points are from healthy subjects and the rest are from cardiac subjects. H represents healthy subjects and P represents congenital heart disease patients. The subject number is reconciled with those in TABLE 1.

A. WAVEFORM IDENTIFICATION RATE

For each subject, the number of valid waveforms associated with heart sound identified within each cardiac cycle over the total number of cardiac cycles among the SCG testing data is calculated as an indicator of the performance of the waveform identification algorithm. Fig. 5 shows the identification rate of the first and second waveform separately. The first seven data are from the seven healthy subjects and the following eleven data are from patients with cardiac disease. The average identification rate over the 18 subjects for the first waveform is 78.8%, and 67.5% for the second waveform. The algorithm performed poorly for the sixth healthy subject due to the noisy SCG data. Of the 17 other subjects whose waveforms were identified successfully, 15 had higher identification rates for the $SS1$ waveform as compared to the $SS2$ waveform. Therefore, in general, the $SS1$ tends to be easier to identify, perhaps because the intensity of the $SS1$ is generally stronger, and the range of $SS1$ timing is smaller than that of $SS2$. Also, the quiescent phase in diastole varies more with respect to heart rate variation, and $SS2$ is produced at the end of ventricular systole and leads ventricular diastole, implying a higher level of variability in the timing of $SS2$.

Factors that could affect the rate of identification:

1) The quality of signal. Noisy signals contain more high-frequency components on top of the true signal making it hard to distinguish the high-frequency waveforms.
2) The morphology of the signal itself. Abnormal morphology appears in signals of cardiac patients, which makes the identification process difficult.

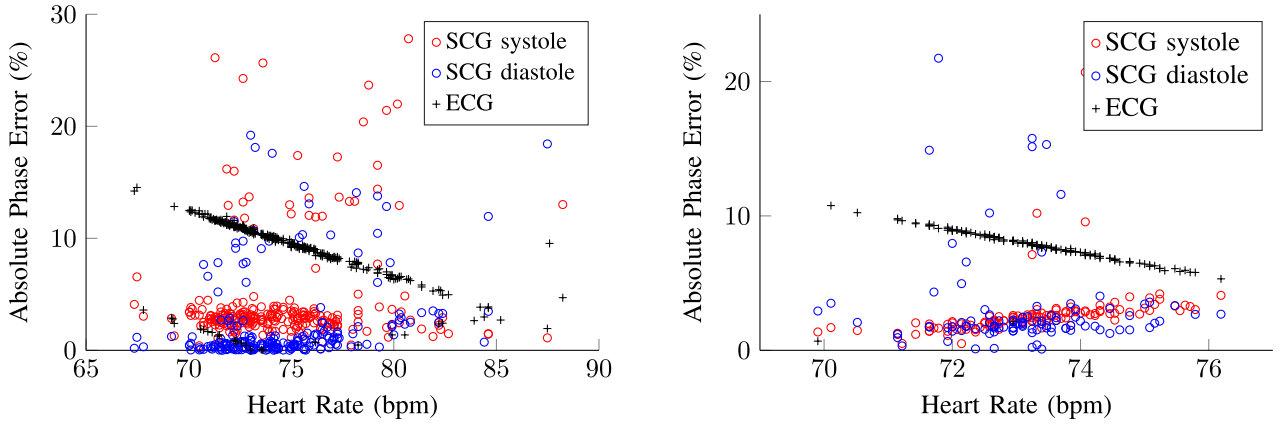

FIGURE 6. Example of absolute phase error versus heart rate of the two heart sound waveforms of SCG and ECG. The left figure is from a healthy subject (subject No. 4), and the right figure is from a cardiac patient (subject No. 14). The absolute phase errors were calculated based on the phase delay function within each cohort.

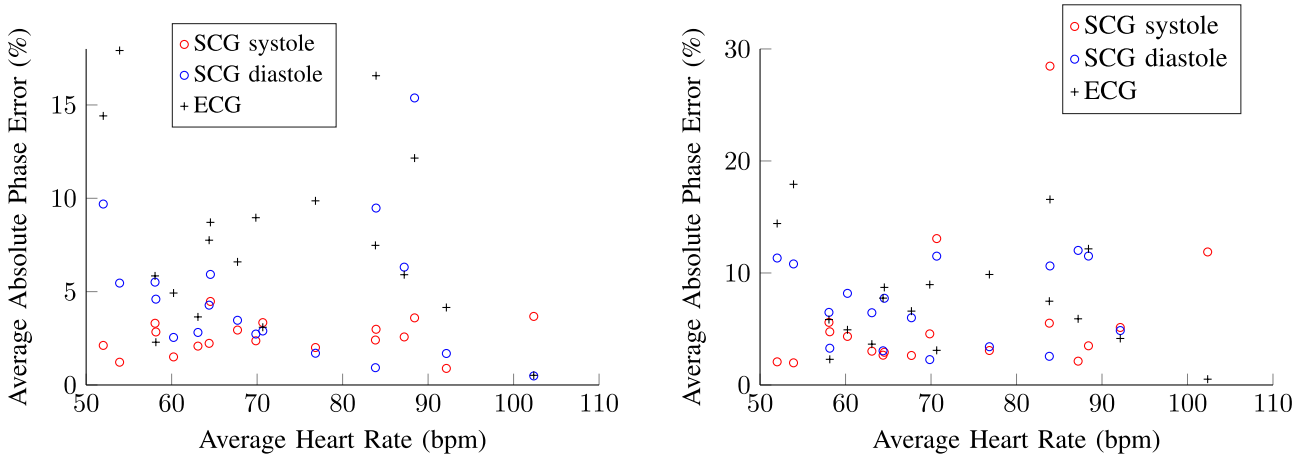

FIGURE 7. Average absolute phase error against average heart rate of all the 18 subjects. The absolute phase errors in the left figure were calculated based on the patient-specific phase delay function, and in the right figure was from each cohort.

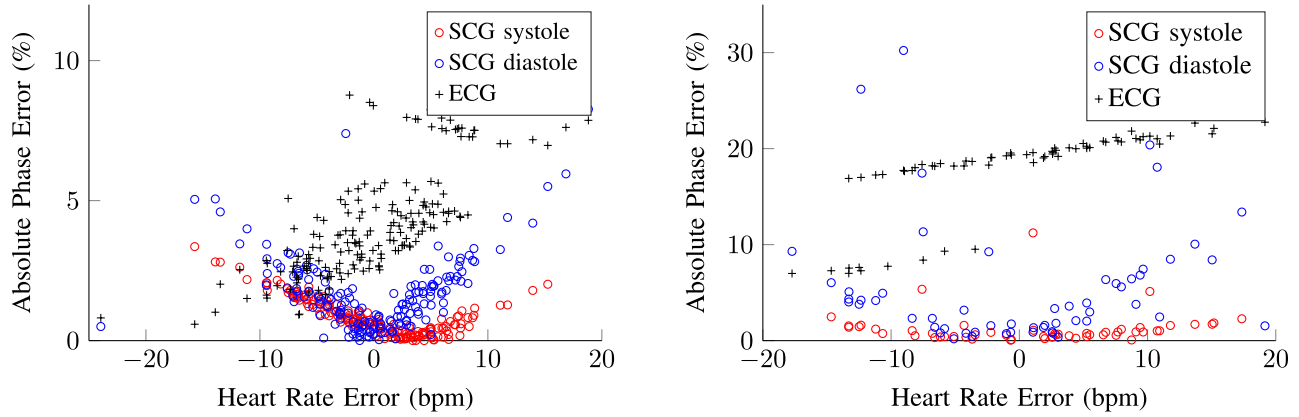

FIGURE 8. Example of absolute phase error versus heart rate error for ECG and the two heart sound waveforms from SCG. The figure on the left is from the a healthy subject (subject No. 7), and the figure on the right is from a cardiac patient (subject No. 9). The absolute phase errors are calculated based on the patient-specific phase delay function.

B. PHASE ERROR VS. HEART RATE

Depicted in Fig. 6 are examples of scatter plots of the phase error with respect to heart rate from a healthy subject and one patient with heart disease, respectively. The phase delay functions are generated using the cohort-specific phase delay function method. The phase errors are calculated based on

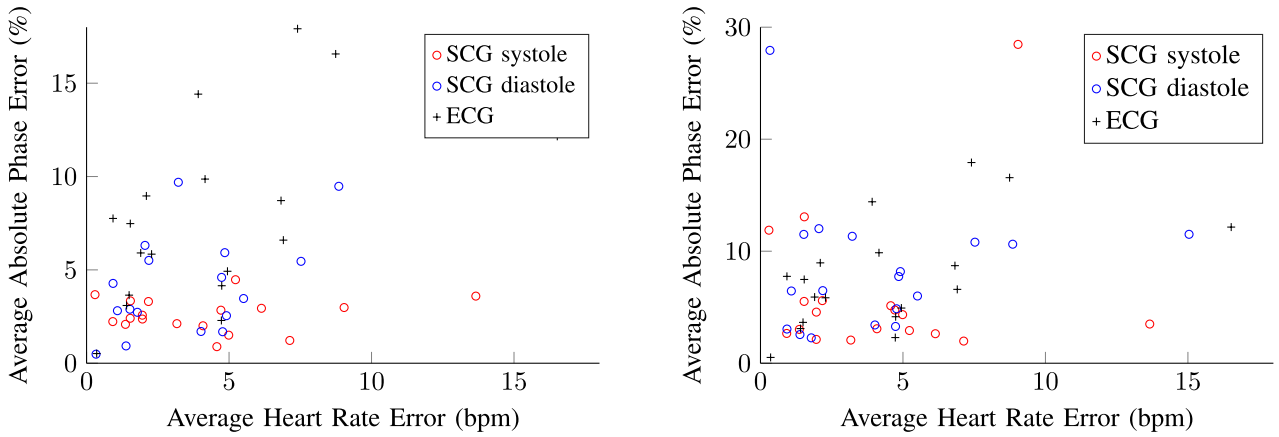

FIGURE 9. Average absolute phase error against average heart rate error of all the 18 subjects. The absolute phase errors on the left are calculated based on the patient-specific phase delay function, and on the right are from each cohort.

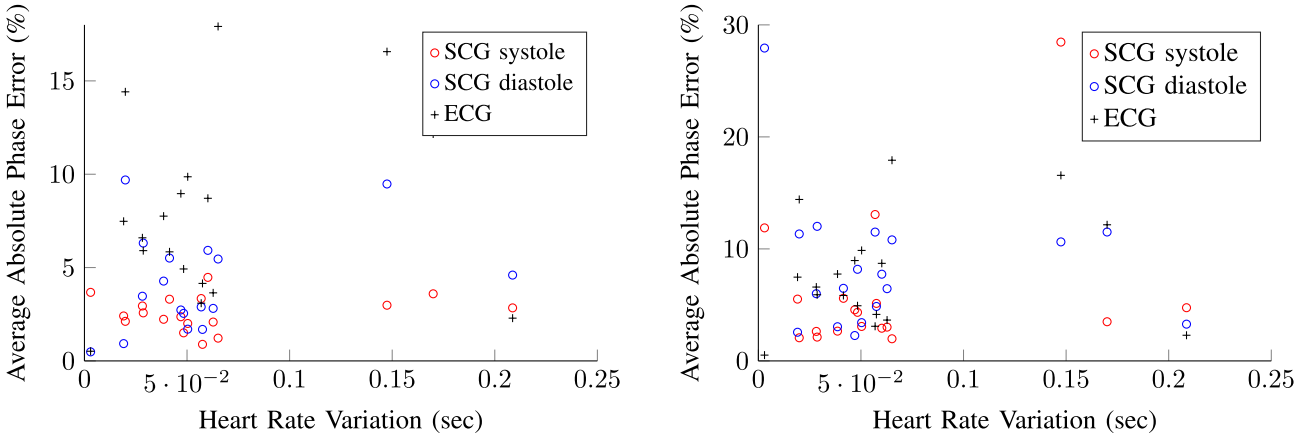

FIGURE 10. Average absolute phase error against average heart rate variation of all the 18 subjects. The absolute phase errors on the left are calculated based on the patient-specific phase delay function, and on the right are from each cohort.

the predicted heart rate, but the horizontal axis shown in the plots represents the true heart rate. The healthy subject shown in the left of Fig. 6 has a higher heart rate and larger heart rate variation than the cardiac patient shown in the right of Fig. 6. In both plots in Fig. 6, ECG phase error decreases as heart rate increases, indicating that ECG could be a better predictor at higher heart rate. Also, particularly for the cardiac patients, SCG phase error increases as heart rate increases, again indicating that ECG could be a better indicator for high heart rates. However, these results do not imply that SCG is less effective than ECG for predicting cardiac CTA gating. Ultimately the true value of cardiac CTA is in excluding coronary artery disease in low risk patients presenting chest pain and without any known coronary or other heart disease. Our rationale for including patients with structural and valvular heart disease in this research was to enlarge the testing population since we scan several of these patients prior to various interventions. In these two examples, the SCG-predicted phases still demonstrated higher accuracy than ECG-predicted phases, if neglecting the outliers. The first and second waveform had comparable performance in prediction.

Summarized plots of average absolute phase error against average heart rate of all the 18 subjects are shown in Fig. 7. SCG-prediction was generated using the patient-specific phase delay function on the left and was generated using the cohort-specific phase delay function on the right. The average phase errors of SCG-based prediction are generally lower using the patient-specific approach. The $SS1$ waveform overall performs better than that of ECG-based prediction in both patient-specific and cohort-specific approach. The performance of the $SS2$ waveform is comparable to that of ECG.

C. PHASE ERROR VS. HEART RATE ERROR

The predicted phase error is expected to increase as the heart rate error grows. Therefore, the expected plot of phase error against heart rate error for a specific subject is intuitively a V shape centered at zero heart rate error. Note that not all the waveforms associated with heart sounds in SCG were identified successfully, however, the predicted heart rate from each cardiac cycle corresponds to a predicted quiescent phase in the ECG piece-wise constant gating function discussed

in Section II-E. Thus, the number of scatter points indicating phase errors associated with the *SS*1 or *SS*2 waveform is no more than that of ECG in Fig. 8. The SCG-based prediction for both subjects in Fig. 8 similarly exhibit a V-shape. Both figures are generated using the patient-specific phase delay function. The absolute phase error is increased as heart rate error increases when using ECG-based prediction relative to SCG-based prediction.

Figure 9 illustrates summarized plots of the average phase error with respect to the average heart rate error of all the 18 subjects. Plots are generated using the patient-specific phase delay function. The average heart rate error takes the average of the absolute value of heart rate errors. The *SS*1 waveform of SCG provides comparatively better prediction than that of ECG and the *SS*2 waveform. As heart rate error increases, the average phase error becomes much higher by using ECG-based prediction than that of SCG-based prediction.

D. AVERAGE PHASE ERROR VS. HEART RATE VARIATION

Figure 10 shows the impact of heart rate variation on the average phase error. The plots are generated from results of all the 18 subjects, using the patient-specific and cohort phase delay function. SCG-based prediction produces less phase error with the patient-specific phase delay function. The *S*1 waveform of SCG is able to more accurately predict with the cohort-specific phase delay function than ECG-based prediction.

IV. DISCUSSION AND CONCLUSION

A sub-system aimed at combining SCG and ECG for quiescent phase prediction was proposed, and supporting algorithms, including SCG template identification and generation algorithm, voting mechanism for echocardiography, phase delay function and heart rate prediction approach, were presented. Automated feature detection from SCG acceleration signal was implemented via a novel template identification and generation algorithm.

A. SUMMARY

Our results show that SCG in general is a predictor of quiescence; however, when the heart rate increases, ECG-based prediction of quiescence improves. Thus combining SCG and ECG could potentially lead to improved real-time gating for cardiac CTA. It was also expected that when the heart rate is low, triggering in diastole is better; when the heart rate is high, triggering in systole is better. However, the predicted phase errors presented in TABLE 2 did not imply such a pattern. This could be caused by the noise and artifacts in echocardiography and SCG.

B. LIMITATIONS

The primary limitation of this work is that our hardware data acquisition system provides SCG and echocardiography signals in sub-optimal conditions. The high-frequency components of SCG are mixed with high-frequency noise that adds to the difficulty in identifying the waveform of heart sounds. Acquiring data with sensors that are more robust to noise may be able to improve the performance of the SCG-based prediction.

Another limitation is the small number of subjects involved in this pilot study. A larger number of healthy subjects and patients would make the results of this study more generalizable. In addition, the patient population that we did study are not representative of the patients who would benefit from coronary CTA. The diastolic quiescent intervals were identified more accurately with ECG for patients with cardiac disease in our cohort. However, this is not considered a significant drawback of potentially gating with SCG. The value of coronary CTA is in ruling out coronary disease in chest pain patients with a low pre-test probability of coronary heart disease. It has been shown in many studies that CTA has very high negative predictive value (93% to 100%). Therefore, cardiac CTA is usually used for evaluating people at low to intermediate risk of coronary artery disease [40]–[42]. Thus, patient for whom the value of coronary CTA is maximized are more likely to be represented by the normal subjects in our cohort. We included patients with non-coronary heart disease in our research because we have a number of such patients who obtained retrospective cardiac scans for other reasons and not to rule out coronary heart disease. So their results do not imply that SCG works worse than ECG. However, it is worth pointing out that among the eleven cardiac patients, three (subject No. 16, 17 and 18) had left ventricular ejection fraction less than 40%. The waveform identification algorithm is able recognize a reasonable number of heart sound-associated waveforms from them.

Furthermore, since the average waveform template is generated based on the buffered data before the CTA scan, when the morphology of cardiac signals differ significantly during data acquisition in real time, for example, heart rate and cardiac signal morphology would change after contrast injection, the template matching method could fail or produce large phase error in predicting quiescence. Lastly, when using a cohort phase delay function, a few outliers could make a big difference in the robustness of the proposed prediction method using SCG. This effect can be minimized by generating a more generalized phase delay function from a larger population.

C. FUTURE WORK

The ultimate goal is to design and implement an automated system that intelligently switches between ECG and SCG for CTA gating. The potential effect of SCG for CTA gating in terms of image quality, feasibility and cost will require further consideration in future research. In addition, comparing the predicted quiescent phase from the proposed algorithm with the observations from CTA data from the corresponding subject to assess the accuracy is expected in future work. This needs to be performed in patients who obtain coronary CTA specifically to evaluate for coronary artery disease. Moreover, the SCG performance could be estimated prior to CTA using

approximately 1-2 minutes of data acquired while patient is on the CT table. Future work should be able to adaptively update the template by using the most recent cardiac cycles. Eventually, the prediction model needs to be implemented in real-time.

ACKNOWLEDGMENT

The authors would like to thank the radiology technologists of the Department of Radiology and Imaging Sciences, Emory University Hospital for their time and assistance in data acquisition. Additionally, the authors appreciate the reviewers for their beneficial critiques and comments. The content is solely the responsibility of the authors and does not necessarily represent the official views of the National Institutes of Health.

REFERENCES

[1] D. Mozaffarian, "Heart disease and stroke statistics—2015 update: A report from the American heart association," *Circulation*, vol. 131, no. 24, pp. e29–e322, 2015.

[2] M. Tavakol, S. Ashraf, and S. J. Brener, "Risks and complications of coronary angiography: A comprehensive review," *Global J. Health Sci.*, vol. 4, no. 1, pp. 65–93, 2012.

[3] A. V. G. Bruschke, W. C. Sheldon, E. K. Shirey, and W. L. Proudfit, "A half century of selective coronary arteriography," *J. Amer. College Cardiol.*, vol. 54, no. 23, pp. 2139–2144, 2009.

[4] B. Desjardins and E. A. Kazerooni, "ECG-gated cardiac CT," *Amer. J. Roentgenol.*, vol. 182, no. 4, pp. 993–1010, 2004.

[5] J. A. Ladapo *et al.*, "Clinical outcomes and cost-effectiveness of coronary computed tomography angiography in the evaluation of patients with chest pain," *J. Amer. College Cardiol.*, vol. 54, no. 25, pp. 2409–2422, 2009.

[6] V. L. Priest, P. A. Scuffham, R. Hachamovitch, and T. H. Marwick, "Cost-effectiveness of coronary computed tomography and cardiac stress imaging in the emergency department: A decision analytic model comparing diagnostic strategies for chest pain in patients at low risk of acute coronary syndromes," *JACC, Cardiovascular Imag.*, vol. 4, no. 5, pp. 549–556, 2011.

[7] M. Rief, S. Feger, P. Martus, M. Laule, M. Dewey, and E. Schönenberger, "Acceptance of combined coronary CT angiography and myocardial CT perfusion versus conventional coronary angiography in patients with coronary stents—Intraindividual comparison," *PLoS ONE*, vol. 10, no. 9, p. e0136737, 2015.

[8] C. A. Wick *et al.*, "Characterization of cardiac quiescence from retrospective cardiac computed tomography using a correlation-based phase-to-phase deviation measure," *Med. Phys.*, vol. 42, no. 2, pp. 983–993, Feb. 2015.

[9] C. A. Wick, O. T. Inan, P. Bhatti, and S. Tridandapani, "Relationship between cardiac quiescent periods derived from seismocardiography and echocardiography," in *Proc. 37th Annu. Int. Conf. IEEE Eng. Med. Biol. Soc. (EMBC)*, Aug. 2015, pp. 687–690.

[10] C. A. Wick *et al.*, "A system for seismocardiography-based identification of quiescent heart phases: Implications for cardiac imaging," *IEEE Trans. Inf. Technol. Biomed.*, vol. 16, no. 5, pp. 869–877, Sep. 2012.

[11] C. A. Wick, O. T. Inan, J. H. McClellan, and S. Tridandapani, "Seismocardiography-based detection of cardiac quiescence," *IEEE Trans. Biomed. Eng.*, vol. 62, no. 8, pp. 2025–2032, Aug. 2015.

[12] Z. Sun, "Coronary ct angiography with prospective ECG-triggering: An effective alternative to invasive coronary angiography," *Cardiovascular Diagnosis Therapy*, vol. 2, no. 1, pp. 28–37, 2012.

[13] S. Mao, M. J. Budoff, L. Bin, and S. C. K. Liu, "Optimal ECG trigger point in electron-beam CT studies: Three methods for minimizing motion artifacts," *Acad. Radiol.*, vol. 8, no. 11, pp. 1107–1115, Nov. 2001.

[14] S. Achenbach *et al.*, "Noninvasive coronary angiography by retrospectively ECG-gated multislice spiral CT," *Circulation*, vol. 102, no. 23, pp. 2823–2828, 2000.

[15] L. Husmann *et al.*, "Coronary artery motion and cardiac phases: Dependency on heart rate—Implications for CT image reconstruction," *Radiology*, vol. 245, no. 2, pp. 567–576, 2007.

[16] H. Seifarth *et al.*, "Optimal systolic and diastolic reconstruction windows for coronary CT angiography using dual-source CT," *Amer. J. Roentgenol.*, vol. 189, no. 6, pp. 1317–1323, 2007.

[17] S. Achenbach, V. Delgado, J. Hausleiter, P. Schoenhagen, J. K. Min, and J. A. Leipsic, "SCCT expert consensus document on computed tomography imaging before transcatheter aortic valve implantation (TAVI)/transcatheter aortic valve replacement (TAVR)," *J. Cardiovascular Comput. Tomogr.*, vol. 6, no. 6, pp. 366–380, 2012.

[18] P. A. Araoz *et al.*, "Optimal image reconstruction phase at low and high heart rates in dual-source CT coronary angiography," *Int. J. Cardiovascular Imag.*, vol. 25, no. 8, pp. 837–845, Dec. 2009.

[19] S. Tridandapani, J. B. Fowlkes, and J. M. Rubin, "Echocardiography-based selection of quiescent heart phases: Implications for cardiac imaging," *J. Ultrasound Med.*, vol. 24, no. 11, pp. 1519–1526, 2005.

[20] C. A. Wick, W. F. Auffermann, A. J. Shah, O. T. Inan, P. T. Bhatti, and S. Tridandapani, "Echocardiography as an indication of continuous-time cardiac quiescence," *Phys. Med. Biol.*, vol. 61, no. 14, p. 5297, 2016.

[21] J. M. Felner, "The first heart sound," in *Clinical Methods: The History, Physical, and Laboratory Examinations*, 3rd ed. Boston, MA, USA: Butterworths, 1990. [Online]. Available: https://www.ncbi.nlm.nih.gov/books/NBK333/

[22] P. Castiglioni *et al.*, "Cardiac sounds from a wearable device for sternal seismocardiography," in *Proc. Annu. Int. Conf. IEEE Eng. Med. Biol. Soc.*, Aug. 2011, pp. 4283–4286.

[23] D. M. Salerno and J. Zanetti, "Seismocardiography for monitoring changes in left ventricular function during ischemia," *CHEST J.*, vol. 100, no. 4, pp. 991–993, 1991.

[24] R. S. Crow, P. Hannan, D. Jacobs, L. Hedquist, and D. M. Salerno, "Relationship between seismocardiogram and echocardiogram for events in the cardiac cycle," *Amer. J. Noninvasive Cardiol.*, vol. 8, no. 1, pp. 39–46, 1994.

[25] M. J. Tadi, T. Koivisto, M. Pänkäälä, and A. Paasio, "Accelerometer-based method for extracting respiratory and cardiac gating information for dual gating during nuclear medicine imaging," *J. Biomed. Imag.*, vol. 2014, Jan. 2014, Art. no. 6.

[26] F. Khosrow-Khavar, K. Tavakolian, and C. Menon, "Moving toward automatic and standalone delineation of seismocardiogram signal," in *Proc. 37th Annu. Int. Conf. IEEE Eng. Med. Biol. Soc. (EMBC)*, Aug. 2015, pp. 7163–7166.

[27] A. Akhbardeh *et al.*, "Comparative analysis of three different modalities for characterization of the seismocardiogram," in *Proc. Annu. Int. Conf. IEEE Eng. Med. Biol. Soc.*, Sep. 2009, pp. 2899–2903.

[28] J. Neary, D. MacQuarrie, and V. Gebhardt, "Relationship between seismocardiography and echocardiography for measuring cardiac cycle timing events," Physiol. Soc., London, U.K., Tech. Rep. 261, 2011.

[29] D. M. Quarrie and P. Neary. (2011). *Comparison of Seismocardiography to Echocardiography for Measuring Cardiac Cycle Events*. [Online]. Available: http://ourspace.uregina.ca/handle/10294/3343

[30] J. M. Zanetti and D. M. Salerno, "Seismocardiography: A technique for recording precordial acceleration," in *Proc. 4th Annu. IEEE Symp. Comput.-Based Med. Syst.*, May 1991, pp. 4–9.

[31] G. D. Clifford, F. Azuaje, and P. McSharry, "ECG statistics, noise, artifacts, and missing data," in *Advanced Methods and Tools for ECG Data Analysis*, vol. 6. London, U.K.: Artech House, 2006, p. 18.

[32] C. Saritha, V. Sukanya, and Y. N. Murthy, "ECG signal analysis using wavelet transforms," *Bulg. J. Phys.*, vol. 35, no. 1, pp. 68–77, 2008.

[33] P. K. Jain, A. K. Tiwari, and V. S. Chourasia, "Performance analysis of seismocardiography for heart sound signal recording in noisy scenarios," *J. Med. Eng. Technol.*, vol. 40, no. 3, pp. 106–118, 2016.

[34] A. Laurin, A. Blaber, and K. Tavakolian, "Seismocardiograms return valid heart rate variability indices," in *Proc. Comput. Cardiol.*, Sep. 2013, pp. 413–416.

[35] F. Khosrow-Khavar, K. Tavakolian, A. P. Blaber, J. M. Zanetti, R. Fazel-Rezai, and C. Menon, "Automatic annotation of seismocardiogram with high-frequency precordial accelerations," *IEEE J. Biomed. health Informat.*, vol. 19, no. 4, pp. 1428–1434, Jul. 2015.

[36] G. Liu, X.-L. Qi, N. Robert, A. J. Dick, and G. A. Wright, "Ultrasound-guided identification of cardiac imaging windows," *Med. Phys.*, vol. 39, no. 6, pp. 3009–3018, 2012.

[37] M. Di Rienzo *et al.*, "Wearable seismocardiography: Towards a beat-by-beat assessment of cardiac mechanics in ambulant subjects," *Auto. Neurosci.*, vol. 178, nos. 1–2, pp. 50–59, Nov. 2013.

[38] J. Reinhold and U. Rudhe, "Relation of the first and second heart sounds to events in the cardiac cycle," *Brit. Heart J.*, vol. 19, no. 4, pp. 473–485, 1957.

[39] Y. S. Abu-Mostafa, M. Magdon-Ismail, and H.-T. Lin, *Learning From Data*, vol. 4. Singapore: AMLBook, 2012.
[40] L. J. Shaw and J. Narula, "Risk assessment and predictive value of coronary artery disease testing," *J. Nucl. Med.*, vol. 50, no. 8, pp. 1296–1306, 2009.
[41] F. Plank *et al.*, "The diagnostic and prognostic value of coronary CT angiography in asymptomatic high-risk patients: A cohort study," *Open Heart*, vol. 1, no. 1, p. e000096, 2014.
[42] M. Shen, N. Saxena, and G. S. Thomas, "Indications and reimbursement of cardiac computed tomography angiography: History, present and future perspectives," *J. Cardiovascular Comput. Tomogr.*, vol. 2, no. 1, pp. 3–11, Jan. 2008.

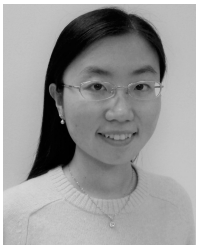

JINGTING YAO (S'13) received the B.E. degree in electrical and computer engineering from the Nanjing University of Posts and Telecommunications, Nanjing, China, in 2014. She is currently pursuing the Ph.D. degree in electrical and computer engineering with the Georgia Institute of Technology, GA, USA.

Her current research is focused on digital signal processing of cardiac signals and development of novel gating strategies for optimizing computed tomography.

SRINI TRIDANDAPANI (S'86–M'95–SM'12) received the B.E. degree in electrical engineering from Anna University, Chennai, India, the M.S.E.E. and Ph.D. degrees in electrical engineering from the University of Washington, Seattle, WA, USA, the M.D. degree followed by residency training in radiology from the University of Michigan, Ann Arbor, MI, USA, the master's degree in clinical and translational research, and the M.B.A. degree from Emory University, Atlanta, GA, USA. After post-doctoral training in computer science with the University of California, Davis, CA, USA, he was an Assistant Professor of Electrical and Computer Engineering with Iowa State University. A boardcertified radiologist, he is currently a Faculty Member with the Department of Radiology and Imaging Sciences, Emory University. He is also an Adjunct Professor with the School of Electrical and Computer Engineering, Georgia Institute of Technology, Atlanta. He received clinical fellowships in cardiothoracic imaging and abdominal imaging with Emory University.

CARSON A. WICK (S'10–M'15) received the B.S., M.S., and Ph.D. degrees in electrical engineering from the Georgia Institute of Technology, Atlanta. During the Ph.D. degree, he completed two Ph.D. Student Internships with the Digitally Enhanced Analog Systems Group, Texas Instruments DSP Research and Development Center, Dallas. After receiving the Ph.D. degree, he served as an Adjunct Researcher with the SWEETLab, Portland State University, where he was involved in systems for remotely monitoring water filtration systems in Africa. After his time in Oregon, he was a Post-Doctoral Fellow with the Department of Radiology and Imaging Sciences, Emory University, where he was involved in developing a complete system for autonomously acquiring point-of-care patient photographs and automatically adding them to the corresponding imaging studies.

He currently serves as the Principal Engineer with Camerad Technologies, LLC, a spin-out from Emory University focused on piloting and refining the technology from his post-doctoral fellowship.

PAMELA T. BHATTI (S'05–M'06) received the B.S. degree in bioengineering from the University of California, Berkeley, CA, USA, in 1989, the M.S. degree in electrical engineering (robotics) from the University of Washington, Seattle, WA, USA, in 1993, the Ph.D. degree in electrical engineering (MEMS) from the University of Michigan, Ann Arbor, MI, USA, in 2006, and the master's degree in clinical research from Emory University in 2013. Before completing the Ph.D. degree, she was with the Department of Radiology, University of Michigan, from 1997 to 1999, where she was involved in the detection of breast cancer with ultrasound imaging. She was with Microware Corporation, Des Moines, IA, USA, from 1996 to 1997, where she was involved in embedded systems software development, Motorola Semiconductor, Austin, TX, USA, from 1994 to 1995, where she was involved in local operating network applications development and customer support, and Alza Corporation, Palo Alto, CA, USA, from 1986 to 1990, where she was involved in the research and fabrication of controlled-release drug delivery systems. She is currently an Associate Professor with the School of Electrical and Computer Engineering, Georgia Institute of Technology, Atlanta, GA, USA. She serves as the Georgia Tech Research, Education, and Career Development Director with the Atlanta Clinical and Translational Sciences Institute, Emory University. In 2011, she received the NSF Career Award to focus on vestibular rehabilitation. Committed to translating technology to the clinical setting, in 2016, she co-founded CameRad Technologies, a company dedicated to improving throughput and quality in radiology imaging.